Three-dimensional solitons in Bose-Einstein condensates with spin-orbit coupling and Bessel optical lattices

Hong Li,[1] Si-Liu Xu,[1,*] Milivoj R. Belić,[2,3] and Jia-Xi Cheng[1]
[1]*School of Electronic and Information Engineering, HuBei University of Science and Technology, Xianning 437100, China*
[2]*Texas A&M University at Qatar, P.O. Box 23874, Doha, Qatar*
[3]*Institute of Physics Belgrade, Pregrevica 118, 11080 Zemun, Serbia*

(Received 27 June 2018; published 26 September 2018)

Applying a variational approach and numerical analysis to the system of Gross-Pitaevskii equations, we find three-dimensional (3D) stable solitons in binary atomic Bose-Einstein condensates with spin-orbit coupling (SOC) and out-of-phase linear and nonlinear Bessel optical lattices. We discuss the stability of 3D solitons by utilizing their norm and energy. The introduction of Bessel potentials makes the evolution and collisions of solitons more stable and improves their resistance to collapse. Depending on the strength of the intra- and intercomponent spatial modulation of the nonlinearity and SOC, we find stable solitons of the semivortex and mixed-mode structures. Furthermore, we show that the solitons are stable against small perturbations in propagation and collisions.

DOI: 10.1103/PhysRevA.98.033827

I. INTRODUCTION

Spatiotemporal localization of waves is a subject which attracts broad interest in physics, spanning such diverse fields as plasma physics, hydrodynamics, nonlinear optics, and Bose-Einstein condensates (BECs). It has been a hot topic in research over the past 20 years, not only theoretically but also experimentally, for example, in various applications of BECs [1–3].

The generation of two-dimensional (2D) and three-dimensional (3D) bright solitons is a significantly more challenging problem than the generation of one-dimensional (1D) solitons. Apart from the obvious advantage that 1D solitons can be treated by the inverse scattering theory, and 2D and 3D solitons cannot, another fundamental difficulty is that the cubic nonlinearity causes the wave collapse in higher-dimensional geometries [4,5]. A number of settings where their stabilization is possible have been proposed. Thus, stable 3D solitons may form in materials with saturable or competing nonlinearities [6,7], nonlocal nonlinearity [8,9], special nonlinear interactions [10,11], optical tandem geometries [12,13], waveguide arrays and optical lattices imprinted in different materials [14–16], and binary BECs subject to the action of spin-orbit coupling (SOC) [17].

The introduction of optical lattices into nonlinear media significantly promoted the stability of localized wave structures in BECs [18,19]. An important concentric axisymmetric optical lattice, the Bessel lattice (BL), has attracted a lot of attention these days. Such a lattice can be induced by the nondiffracting Bessel beams, which can be created in experiments by computer-generated holograms [20] or conical prisms (axicons) [21]. The complex lattices can also be created in photorefractive crystals by the phase-imprinting technique [22,23]. Various types of solitons have been predicted theoretically and observed experimentally in modulated BLs [24,25]. The unique cylindrical symmetry of such a lattice allows for the existence of stable ring-profiled vortex [26], multipole [27], and necklace solitons [28], as well as 2D or 3D spatiotemporal solitons [16,29], provided the lattice is modulated deeply enough.

On the other hand, spin-orbit coupled BECs [30,31], experimentally realized in [32], attracted particular attention not only for allowing one to study phenomena related to the artificial vector gauge potentials [33] but also for giving rise to a number of remarkable structures, such as vortices [34], monopoles [35], multidomain patterns [36], solitons [37,38], and others. In recent years, diverse vortex patterns have been found in BECs with SOC and attractive nonlinearity, trapped in external potentials [17,39,40], which apparently is different from the ones mentioned above. Sakaguchi *et al.* displayed several types of self-trapped vortex-soliton complexes in a 2D model of the binary BEC, with the SOC of Rashba type between the two components and an attractive intrinsic nonlinearity [39]. Kartashov *et al.* introduced SOC in a BEC as a gauge potential, acting only in a localized spatial domain, and discussed the properties of soliton complexes and spinor dynamics [40]. Zhang *et al.* revealed in [17] that the self-attractive binary SOC condensate can support stable 3D solitons in free space, in spite of the fact that the setting has no ground state at any value of the norm. It is shown that the SOC-induced modification of the dispersion of the 3D condensate may balance the attractive nonlinearity, creating metastable solitons.

Despite the above progress, 3D vortex solitons created in such binary condensates by attractive nonlinear interactions and SOC are still inadequately understood, especially when BLs are added. The aim of the present paper is to construct 3D stable solitons in binary atomic condensates with SOC, in combination with out-of-phase linear and

*Corresponding author: xusiliu1968@163.com

nonlinear BLs, by means of a variational approach (VA) and a systematic numerical analysis. The existence of 3D stable solitons featuring a semivortex (SV) or a mixed-mode (MM) structure is demonstrated [17]. Furthermore, it is shown that the solitons are stable in propagation and collisions, depending on the relative strength of SOC and the intra- and intercomponent spatial modulation of the nonlinearity.

II. MODEL AND NUMERICAL METHOD

The system of scaled 3D Gross-Pitaevskii equations for the spinor wave function $\Psi = (\Psi_+, \Psi_-)$ of the binary BEC with attractive contact interactions and the SOC of Rashba type, which is trapped in a BL, can be written as

$$\begin{aligned} i\frac{\partial \Psi_+}{\partial t} + \frac{1}{2}\nabla^2\Psi_+ + i\lambda\left(\frac{\partial \Psi_-}{\partial x} - i\frac{\partial \Psi_-}{\partial y} + \frac{\partial \Psi_+}{\partial z}\right) + g[(1-\delta R)|\Psi_+|^2 + \eta|\Psi_-|^2]\psi_+ + pR\Psi_+ = 0 \\ i\frac{\partial \Psi_-}{\partial t} + \frac{1}{2}\nabla^2\Psi_- + i\lambda\left(\frac{\partial \Psi_+}{\partial x} + i\frac{\partial \Psi_+}{\partial y} - \frac{\partial \Psi_-}{\partial z}\right) + g[(1-\delta R)|\Psi_-|^2 + \eta|\Psi_+|^2]\psi_- + pR\Psi_- = 0 \end{aligned} \tag{1}$$

where λ is the strength of the self-spin coupling in the isotropic form of SOC [38,39], g is the strength of the nonlinear interaction, η is the relative cross-nonlinearity strength, and p and δ describe modulation depths of the linear and nonlinear BLs, respectively. The stationary wave function is of the form $\Psi_\pm = e^{-i\mu t}\psi_\pm$, where μ is the chemical potential. For the lattice, we pick $R = J_n(kr)$ where n is the order of BL. We fix the radial scale to 2 ($k = 2$) and the interaction strength to $g = 1$.

Let $N = \int d\boldsymbol{r}(|\psi_+|^2 + |\psi_-|^2)$ be the norm; the corresponding energy E is

$$\begin{aligned} E = \int d\boldsymbol{r}\Bigg[\frac{1}{2}(|\nabla\psi_+|^2 + |\nabla\psi_-|^2) - i\lambda(\psi_+^*\ \psi_-^*)\boldsymbol{\nabla}\cdot\boldsymbol{\sigma}\begin{pmatrix}\psi_+\\ \psi_-\end{pmatrix} - pR(r)(|\psi_+|^2 + |\psi_-|^2) \\ - \frac{g}{2}(1-\delta R)(|\psi_+|^4 + |\psi_-|^4 + 2\eta|\psi_+\psi_-|^{\,2})\Bigg] \end{aligned} \tag{2}$$

where $\sigma = (\sigma_x, \sigma_y, \sigma_z)$ is the Pauli matrix. On account of the BL being an infinite series, we cannot simply use the dimensional analysis. So, we use the variational method to treat the problem [39,40], in parallel with numerical analysis. In cylindrical coordinates (r, ϕ, z), we choose the following ansatz for the SV and MM structures of the stationary wave function, and we only analyze the state the energy of which is always the lowest, with the integer vorticity zero. The forms of SV and MM are chosen as follows:

$$\text{SV:}\psi_{\text{SV}+} = (A_1 + iB_1 z)e^{-\alpha_1 r^2 - \beta_1 z^2}, \quad \psi_{\text{SV}-} = (iA_2 + B_2 z)re^{-\alpha_2 r^2 - \beta_2 z^2 + i\phi} \tag{3a}$$

$$\text{MM:}\psi_{\text{MM}+} = \cos\theta\,\psi_{\text{SV}+} - \sin\theta\ \psi_{\text{SV}-}{}^*, \quad \psi_{\text{MM}-} = \cos\theta\,\psi_{\text{SV}-} + \sin\theta\ \psi_{\text{SV}+}{}^*. \tag{3b}$$

Now, the relation between the energies of SV and MM can be obtained:

$$E_{\text{MM}} = E_{\text{SV}} + \frac{c}{2}\left\{(1-\eta)\int d\boldsymbol{r}[\Delta E\ \times\ (1-\delta R)]\right\} \tag{4}$$

where $c = 2\sin^2\theta\cos^2\theta$, $\Delta E = |\psi_{\text{SV}+}|^4 + |\psi_{\text{SV}-}|^4 - 4|\psi_{\text{SV}+}\psi_{\text{SV}-}|^2$. Substituting Eq. (3b) into Eq. (2) and taking the derivative of c, one gets $\sin 4\theta = 1$; thus it is required that $\theta = 0.25\pi,\ 0.5\pi,\ 0.75\pi,\ \pi$. As the energy of MM is different from SV when $\eta \neq 1$, we can fix $\theta = 0.25\pi$ and $c = 0.5$. From Eq. (4) one can infer whether the energy of SV or the energy of MM is lower, depending on δ and η; this can be verified by numerical calculation (see Fig. 2). We use Eq. (3) as the initial guess wave in the accelerated imaginary time evolution method (AITEM) [41], to get numerical results. One can take $N = \int d\boldsymbol{r}(|\psi_+|^2 + |\psi_-|^2)$ or $A = |\psi_+|_{\max} + |\psi_-|_{\max}$ as the normalization after every imaginary time evolution step. The original AITEM method is doomed to fail when calculating the left branch in Fig. 1. However, an improved AITEM method invented later is very efficient and could be applied. Comparing AITEM and VA, we find VA to be inaccurate when the Bessel potential is introduced, especially in the cases of higher order ($n > 1$). This is presented in Fig. 1, which depicts the norm of stable solitons as a function of the chemical potential. Hence, our main conclusions come from the full numerical method. As mentioned, in this procedure Eqs. (3) are used as initial guesses.

In order to check the stability of solutions, we perform direct numerical simulation using the split-step Fourier method in real time [42]. We separate the linear operator L in Eq. (5a) and the nonlinear operator $N1$ in Eq. (5b) below:

$$i\frac{\partial}{\partial t}\begin{pmatrix}u\\ v\end{pmatrix} + \frac{1}{2}\nabla^2\begin{pmatrix}u\\ v\end{pmatrix} + i\lambda\nabla\cdot\boldsymbol{\sigma}\begin{pmatrix}u\\ v\end{pmatrix} = 0, \tag{5a}$$

$$i\frac{\partial}{\partial t}\begin{pmatrix}u\\ v\end{pmatrix} + g\begin{pmatrix}(1-\delta R)|u|^2 + \eta|v|^2 & 0\\ 0 & (1-\delta R)|v|^2 + \eta|u|^2\end{pmatrix}\begin{pmatrix}u\\ v\end{pmatrix} + pR\begin{pmatrix}u\\ v\end{pmatrix} = 0. \tag{5b}$$

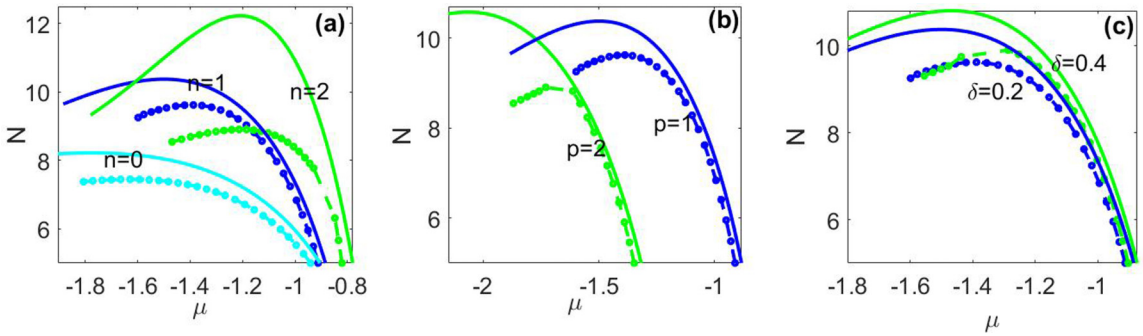

FIG. 1. Three-dimensional stable solitons predicted numerically (dash-dotted lines) and variationally (solid lines) for the MMs when $g = \lambda = 1$. (a) $n = 0, 1, 2$. (b) $n = 1$, and $p = 1, 2$. (c) $n = 1$, and $\delta = 0.2, 0.4$. The stable solitons are the ones with $d\mu/dN<0$, according to the VK criterion.

The propagators e^{N1} and e^{L} are formed by formally solving these partial equations with an initial condition u_0 and v_0 in the frequency domain (see the Appendix). We let them evolve for Δt in time for every step. After taking the Fourier transform, one gets

$$u = C_1 e^{iq_1\Delta t} + C_2 e^{iq_2\Delta t}, \quad v = C_3 e^{iq_1\Delta t} + C_4 e^{iq_2\Delta t} \tag{6}$$

where $q_{1,2} = \frac{-w^2 \pm 2\lambda w}{2}$, $C_{1,2} = \frac{u_0 w \mp v_0(w_x - iw_y) \mp w_z u_0}{2w}$, $C_{3,4} = \frac{v_0 w \mp u_0(w_x + iw_y) \pm w_z v_0}{2w}$, and $w = \sqrt{w_x^2 + w_y^2 + w_z^2}$ is the Fourier frequency. The results are discussed in the following sections.

III. SOLITARY MODES OF SV AND MM

First, in Fig. 1 the stable 3D solitons are predicted for MMs with different orders n, the modulation depths of the linear p, and the nonlinear δ of BL, by both VA and AITEM. One can see that the norm N reaches the maximum value at a certain μ, which is defined as $N_{\max}$. For smaller μ, the positive slope of the dependence $d\mu/dN>0$ can be observed. It does not satisfy the Vakhitov-Kolokolov (VK) criterion [6], thus the solitons there are unstable. In contrast, when μ becomes larger, the stable solitons can be seen in Fig. 1, as well as in Figs. 4 and 6. Further, it is seen that $N_{\max}$ is bigger at $n = 1$ than at $n = 0$ or 2. We also numerically calculate the energy for $n = 0, 1, 2, 3$ with $n = 7$, $\delta = 0.2$, $p = 1$. It is found that the energies for $n = 0, 1$ are similar and lower than for $n = 2, 3$ (the energies are -6.1823, -6.1806, -5.6575, -5.4304 for $n = 0, 1, 2, 3$, respectively). In Figs. 1(b) and 1(c), one can see that N decreases as the linear modulation depth of the BL p increases. Otherwise, N increases as δ increases. For fixed λ, η, δ, and p, the stable solitons always exist in a finite interval of the norm $0 < N < N_{\max}$. There is no minimum norm for the appearance of the solitons—they exist all the way up to $N_{\max}$; this conclusion is similar to [17], but there it is obtained in free space. In addition, from Fig. 1 one can see that AITEM is in better agreement with the prediction of the VA at bigger μ. The unstable branch from the VA, however, can be produced by AITEM, which is different from [17].

In Figs. 2(a) and 2(b), we calculate energy for varying η. One can see that the energy of $n = 0$ is bigger than that of $n = 1$ at the same η, and the higher-order BLs are more likely to form stable patterns than the lower-order ones. In addition, there exists a critical value $\eta_{\rm cr} = 0.82, 0.92$, at which the energies of SV and MM become equal. In Fig. 2(c), we calculate $\eta_{\rm cr}$ for different δ; obviously, δ strongly affects this value. The energy of MM when $\delta>(1-\eta)/0.4$ is lower than that of the SV, and vice versa for $\delta<(1-\eta)/0.4$. In Figs. 2(d)–2(f), we display the energy for different parameters δ, p, and N. In Fig. 2(d), one can see that increasing the depth of the nonlinearity modulation δ results in a significant growth of the maximum energy that solitons can carry, where the energy of SV is bigger than that of MM, whereas, as p increases, the energy decreases, as can be seen in Fig. 2(e). In Fig. 2(f), the corresponding norm-energy diagram exhibits a single cusp, connecting the branches where the derivative $d\mu/dN$ is negative [the lower curve on the $N(\mu)$ diagram] or positive [the upper curve on the $N(\mu)$ diagram]. It is a well-established fact that in BLs with uniform or anisotropic nonlinearity the branches with $d\mu/dN<0$ correspond to stable solutions, in accordance with the VK stability criterion.

Figure 3 shows the maximum norm $N_{\max}$ versus different p, δ, and λ, for the MM. In Fig. 3(a), it is seen that $N_{\max}$ generally decreases as the strength p of BLs increases; thus, the linear modulation depth p causes the stabilization of solitons. However, increasing p does not always cause a decrease in $N_{\max}$, and there might exist a $p_{\rm cr}$ value where $N_{\max}$ reaches an extremum locally. It is certificated that if $p = \delta = 0$, that is, without BLs, the SOC can also protect 3D solitons from collapse [17]. Increasing δ causes a significant increase of $N_{\max}$. Figure 3(c) shows that there exists $N_{\max}$ even though $\lambda = 0$, which is the case of the sole BEC with BLs and attractive contact interactions. As a result, the maximum critical value $N_{\max} = 14$ can be obtained. Furthermore, one can make a conclusion that $N_{\max}$ decreases as the strength λ of SOC increases, which is satisfied for $0\leqslant\lambda\leqslant 1$.

The prediction for the existence of stable 3D solitons in free space calls for verification by direct numerical simulation of Eq. (4). We display stationary states by simulating in imaginary time. In Figs. 4(a)–4(d), we show the stable 3D wave density distributions of SV and MM in BLs, for $\eta = 1$, $N = 7$, $\lambda = 1$, $p = 1$, and $\delta = 0.2$. This corresponds to two

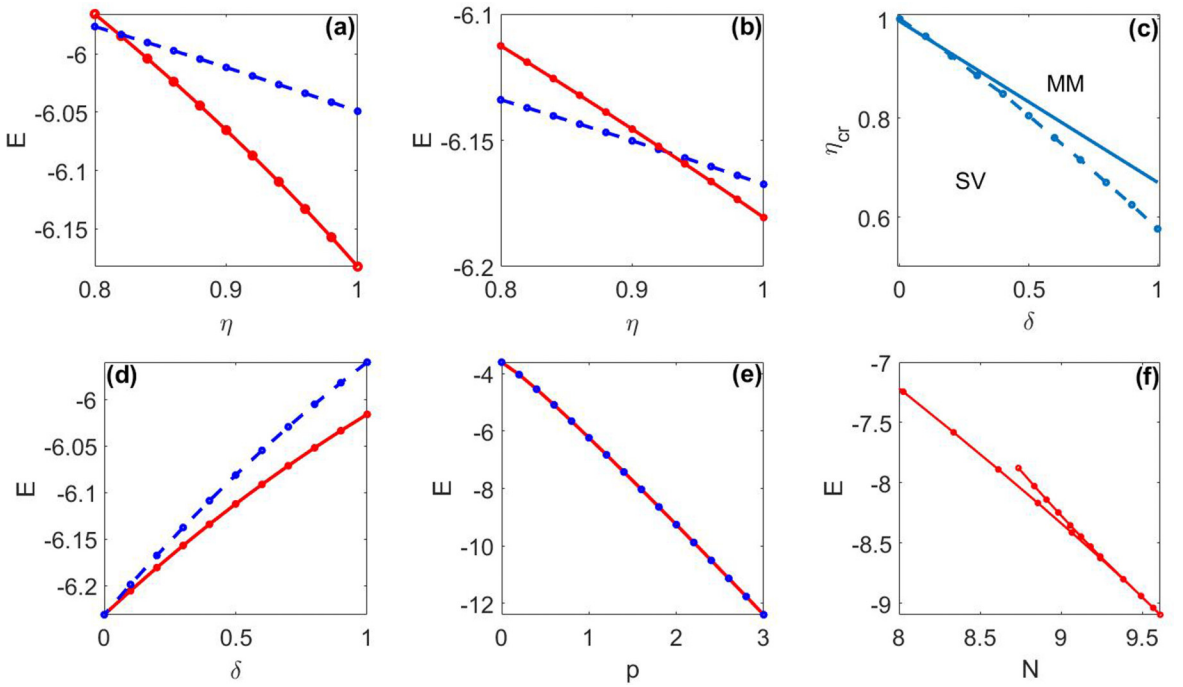

FIG. 2. (a) Energies vs the relative cross-nonlinearity strength η with $N = 7$, $\lambda = 1$, $g = 1$, $p = 1$, $\delta = 0.2$, $n = 0$ for SV (the blue dot-dashed line) and MM (the red dot-solid line). (b) Same as panel (a) but with $n = 1$. (c) η_{cr} vs δ when $E_{SV} = E_{MM}$. (d–f) Energy vs δ, p, and N. (d) $N = 7$, $\lambda = 1$, $g = 1$, $p = 1$, $n = 1$. (e) $N = 7$, $\lambda = 1$, $g = 1$, $\delta = 0.2$, $n = 1$. (f) $\lambda = 1$, $g = 1$, $p = 1$, $\delta = 0.2$, $n = 1$.

solid dots D (red, MM) and F (blue, SV) in Fig. 4(f), which depicts energy as a function of the width L, defined below. The asymmetry of the MM solitary package originates from the interaction of the nonlinear intra- and interspecies and the vortex in an axisymmetric BL, which is different from [17]. Furthermore, one can infer that the density distributions of SV are axisymmetric, while the two pseudospin wave functions ψ_+ and ψ_- are mirror symmetric for MM.

After performing direct numerical propagation of the stable stationary solutions, one can infer that the numerical solutions generally retain input shapes and stay close to the stable solutions, even under considerable perturbation. On the other hand, the unstable solitons gradually lose axisymmetry or mirror symmetry, and move away from the input shapes without perturbation, but still are more likely not to collapse than in the free space.

In order to look more closely into the stability when N is considered, we define the characteristic size of the condensate $L = \int d\boldsymbol{r}[(|\psi_+|^2 + |\psi_-|^2)|\boldsymbol{r}|]/N$, and then make the conversion of variables $\psi_\pm = A\psi_\pm$, $x = A^{-2/3}x$, $y = A^{-2/3}y$, $z = A^{-2/3}z$. From numerical solutions in Figs. 4(a)–4(d), one can calculate the corresponding sizes $L = 1.41$ (MM) and *1.60* (SV) in Fig. 4(f) (dots D and F). In Figs. 4(e) and 4(f), it is shown that the bigger δ the bigger the characteristic size L and the energy E of the numerical solution. On the other hand, the bigger p makes them decrease (dots A–D, F). The dots are located at the local minimum points of the curves, and the characteristic size of the condensate L at $p = 0$ is longer than that in the linear Bessel potential at $p > 0$. Hence, it is clear that the solitons become more stable when p is nonzero.

IV. COLLISIONS OF VORTEX MODES

In the following, we consider the collision of solitons. To construct solitons moving along the z axis with velocity V_z, we introduce the traveling-wave variable

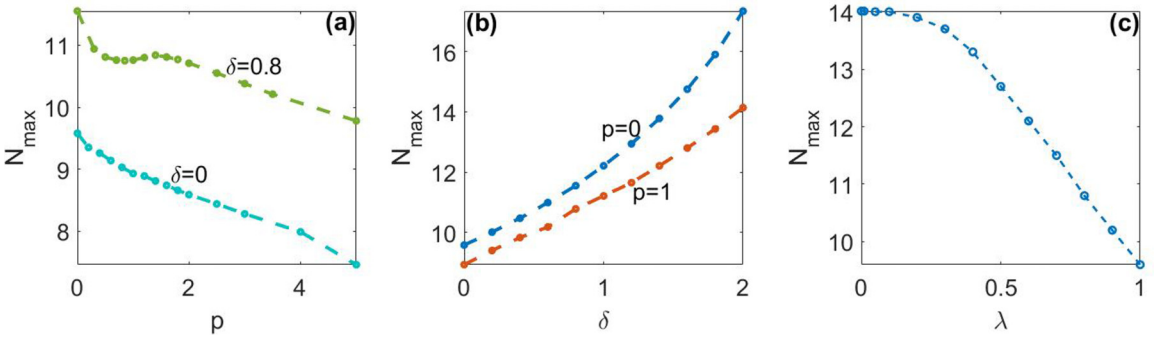

FIG. 3. Maximum norm N_{max} vs different p, δ, and λ for MM. (a) $\delta = 0, 0.8$. (b) $p = 0, 1$. (c) $\delta = 0.2$, $p = 1$.

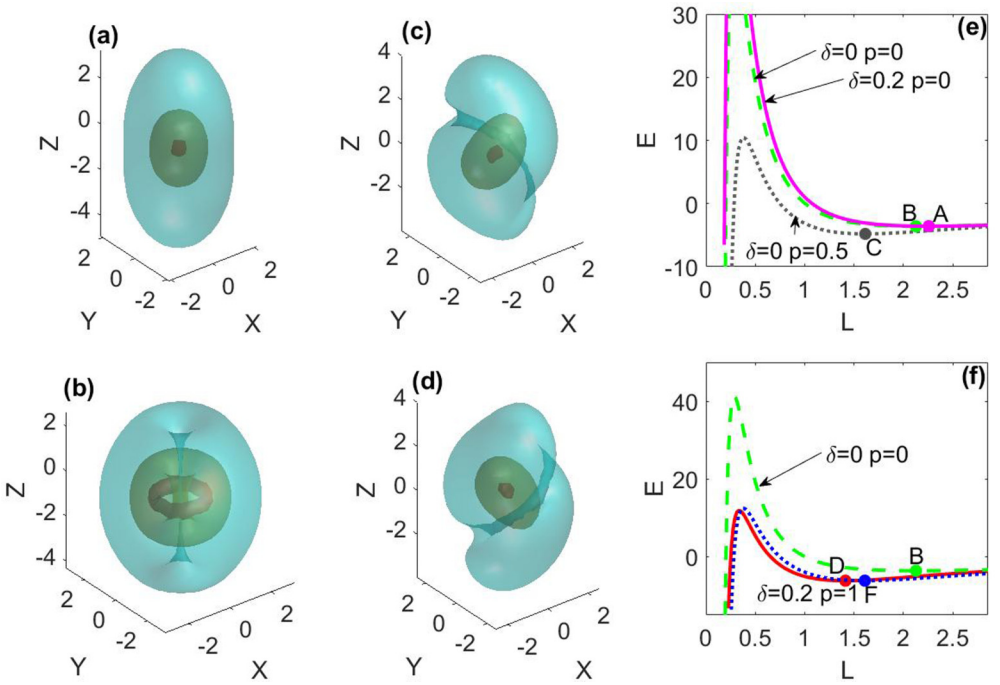

FIG. 4. Soliton density profile for $\eta = 1$, $N = 7$, $\lambda = 1$, $p = 1$, $\delta = 0.2$. (a, b) SV. (c, d) MM. Different colors represent constant-magnitude surfaces $(0.95,\ 0.5,\ 0.06)\ \times |\psi_{\pm}|_{\max}$ from the inner to the outer. (e, f) Energy vs the characteristic size of MM and SV. Solid dots (A, B, C, D, F) of different colors are local minima of the curves for MM or SV. The purple solid line (A) is for $p = 0$, $\delta = 0.2$; the green dashed line (B) is for $p = 0$, $\delta = 0$; the gray dotted line (C) is for $p = 0.5$, $\delta = 0$. The red solid line (D) represents MM and the blue dotted line (F) represents SV.

$\psi_{\pm} = \psi_{\pm}(x, y, z - V_z t)$; that is, we rewrite and solve Eq. (1) in the moving frame of reference. In Figs. 5(a) and 5(b), we plot the ratio of spin populations as functions of V_z. We choose MM with $\eta = 1$, $p = 1.5$, $\sigma = 0.8$, $N = 10$, $n = 1$ at initial positions $z_0 = \pm 10$. In this form, the velocity term affects the SOC strength and the BL strength along the z axis, breaking the symmetry between the two components of the spinor. As a result, the positive (negative) V_z tends to increase the population of the spin-down (-up) component. Further increasing V_z in the positive or negative direction could transform the state of lower energy from MM to SV. In the negative direction, the critical value of V_z is between -0.05 and -0.1, while in the positive direction it is between 0.05 and 0.1. This could force one component to vanish, so that Eq. (1) could be simplified into the single BEC with an attractive contact interaction and BL. When V_z is too large, we cannot find a soliton solution, which means V_z can also affect $N_{\max}$.

Figures 5(c), 5(d), and 6 display the collision of SV between two spin-up (down) solitons trapped in an additive potential $0.5\Omega^2(x^2 + y^2 + z^2)$, with the trapping frequency Ω used to control the velocity in collision. In Figs. 5(c) and 5(d), the peak positions of soliton pairs are shown along the z axis varying in time, and the detailed process of collision is depicted in Fig. 6. It is seen that the slowly moving solitons undergo a quasielastic collision in Figs. 6(a) and 6(b), while in Figs. 6(c) and 6(d), after increasing the trapping frequency to $\Omega = 1.5$, the collision is a bit smeared. Unlike in the free space [17], the collision does not lead to the destruction of faster solitons ($V_z = 1.4$) under BLs, and the soliton collision is more localized.

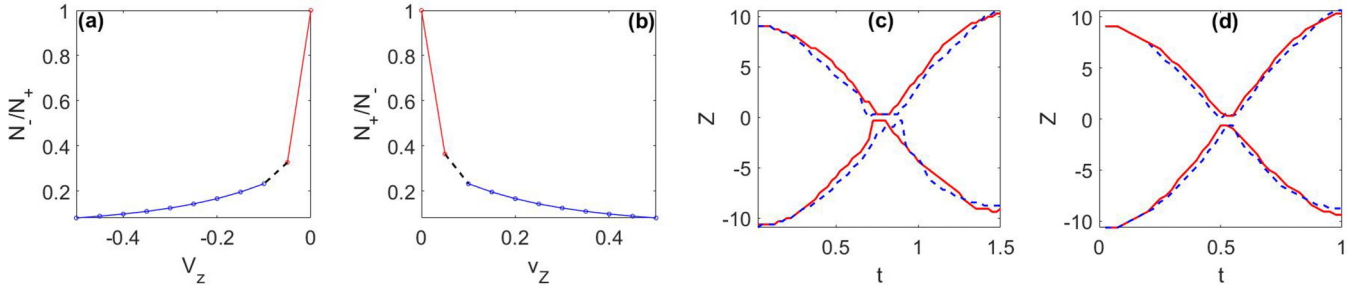

FIG. 5. (a, b) The ratio of spin populations as a function of velocity V_z for the moving SV with $\eta = 1$, $\lambda = 1$, $p = 1.5$, $\delta = 0.8$, $N = 10$, $n = 1$, and $N_{\pm} = \int dr(|\psi_{\pm}|^2)$. The red line represents MM, and the blue line represents SV, separated by the black dashed line. (c, d) Peak positions of ψ_+ (dashed blue) and ψ_- (red) along the z axis varying in time, for $\Omega = 1$ and 1.5.

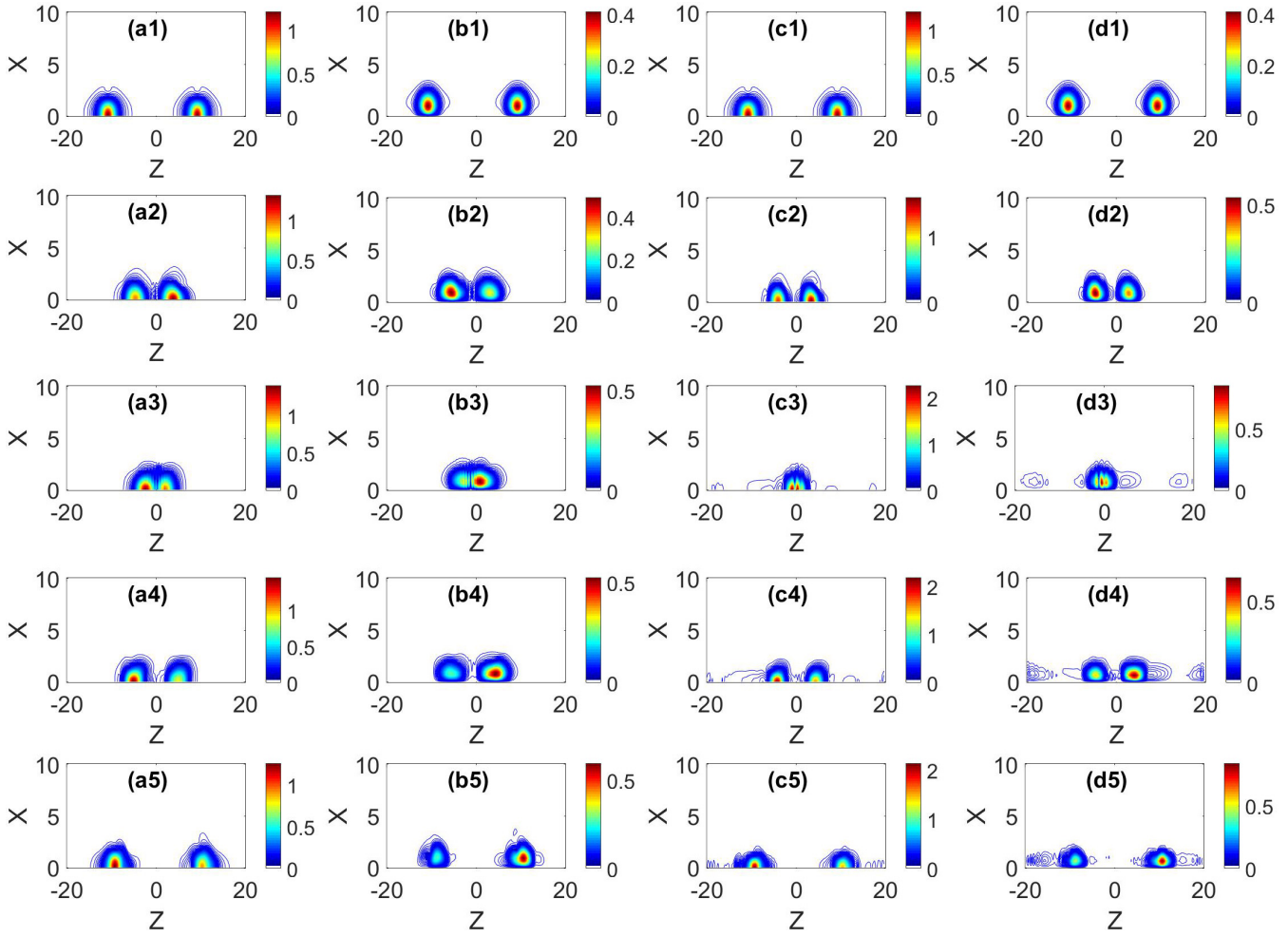

FIG. 6. Collisions of stable 3D SVs for $\Omega = 1$. (a1) The initial ($t = 0$) 3D density profile of the spin-up components (ψ_+). (a1–a5) The process of collision seen through a cross-section at $y = 0$ and $t = 0$, 0.575, 0.9, 1.05, 1.5, respectively. (b1–b5) The spin-down components (ψ_-). (c1–c5, d1–d5) The same as panels (a1)–(a5), (b1)–b(5) but for $\Omega = 1.5$, at $t = 0$, 0.4, 0.55, 0.675, 1.

V. CONCLUSION

We have studied the 3D solitons in BECs with spin-orbit coupling and linear and nonlinear Bessel lattices. The combination of analytical and numerical methods reveals that stable 3D solitons can be supported in the binary atomic condensate with attractive interactions, with properly engineered SOC and with out-of-phase linear and nonlinear BLs. This is an example of stable solitons in the 3D inhomogeneous environment with local cubic self-attraction and without a ground state in the system. The introduction of Bessel potentials makes the evolution and collisions of solitons more stable and improves their resistance to collapse. In three dimensions, the existence of stable solitons is controlled not only by the norm but also by the energy, as the above analysis clearly shows. In particular, the relative strength of the SOC and the intra- and intercomponent spatial modulation of nonlinearity plays an essential role for the stabilization of solitons in propagation and collision.

ACKNOWLEDGMENTS

This work is supported in China by the National Natural Science Foundation of China (Grants No. 11747044 and No. 11747044), Hubei Provincial Department of Education (Grant No. B2017063), Hubei Province Science and Technology Support Program (Grants No. 2015BAA001 and No. 2015CFC779), Hubei SMEs Innovation Fund Project (Grant No. 2015DAL069), and Dr. Start-up fund (Grant No. BK1427). In addition, work in Qatar is supported by NPRP Project No. 8-028-1-001 with the Qatar National Research Fund and in China by the Natural Science Foundation of Guangdong Province (Grant No. 1015283001000000). M.R.B. also acknowledges support from the Al Sraiya Holding Group.

APPENDIX

After taking the Fourier transform, we can write Eq. (5a) as follows:

$$i\frac{\partial u}{\partial t} - \tfrac{1}{2}w^2 u + \lambda(-w_x v + i w_y v - w_z u) = 0, \quad \text{(A1a)}$$

$$i\frac{\partial v}{\partial t} - \tfrac{1}{2}w^2 v + \lambda(-w_x u - i w_y u + w_z v) = 0 \quad \text{(A1b)}$$

where w_x, w_y, and w_z are the Fourier frequencies, and $w = \sqrt{w_x^2 + w_y^2 + w_z^2}$. Then one can easily find

$$v = \frac{i\frac{\partial u}{\partial t} - \frac{1}{2}w^2 u - \lambda w_z u}{\lambda w_x - i\lambda w_y}, \quad u = \frac{i\frac{\partial v}{\partial t} - \frac{1}{2}w^2 v + \lambda w_z v}{\lambda w_x + i\lambda w_y}. \tag{A2}$$

We can choose the first of the above two equations, Eq. (A2), to substitute into Eq. (A1b), or choose the second one to substitute into Eq. (A1a); in both cases, one obtains the same second-order linear differential equation for either u or v:

$$\frac{\partial^2 u}{\partial t^2} + iw^2\frac{\partial \mathrm{u}}{\partial \mathrm{t}} + \left(\lambda^2 w^2 - \frac{1}{4}w^4\right)u = 0. \tag{A3}$$

This is a simple second-order ordinary differential equation. The corresponding characteristic equation is

$$q^2 + iw^2 q + \lambda^2 w^2 - \tfrac{1}{4}w^4 = 0. \tag{A4}$$

The two solutions of Eq. (A4) are $q_1 = (-\mathrm{w}^2 + 2\lambda w)/2$, $q_2 = (-\mathrm{w}^2 - 2\lambda w)/2$. Thus, the general solution of Eq. (A3) is of the form $u = C_1 e^{iq_1\Delta t} + C_2 e^{iq_2\Delta t}$, $v = C_3 e^{iq_1\Delta t} + C_4 e^{iq_2\Delta t}$. With an initial condition u_0 and v_0 in the frequency domain, one can substitute it into Eqs. (A1a) and (A1b); then C_1, C_2, C_3, and C_4 as functions of u_0, v_0, w_x, w_y, w_z, and w [Eq. (A5e)] can be found from Eqs. (A5a)–(A5d):

$$C_1 + C_2 = u_0, \tag{A5a}$$

$$C_3 + C_4 = v_0, \tag{A5b}$$

$$-C_1(w + w_z) = (w_x - iw_y)C_3, \tag{A5c}$$

$$C_2(w - w_z) = (w_x - iw_y)C_4, \tag{A5d}$$

$$C_{1,2} = \frac{u_0 w \mp v_0(w_x - iw_y) \mp w_z u_0}{2w},$$

$$C_{3,4} = \frac{v_0 w \mp u_0(w_x + iw_y) \pm w_z v_0}{2w}. \tag{A5e}$$

To avoid dividing with $w = 0$ in Eq. (A5e), we replace zero by a very small number. The analytical solution avoids diagonalization of a matrix for numerical solution, which is a difficult task for a computer, especially in three dimensions. In this manner, we are able to utilize the split-step Fourier method with higher accuracy and bigger Δt.

[1] P. G. Kevrekidis, D. J. Frantzeskakis, and R. Carretero-Gonzalez, *Emergent Nonlinear Phenomena in Bose-Einstein Condensates: Theory and Experiment* (Springer, New York, 2008), p. 157.

[2] A. L. Fetter, Rev. Mod. Phys. **81**, 647 (2009).

[3] B. Eiermann, Th. Anker, M. Albiez, M. Taglieber, P. Treutlein, K.-P. Marzlin, and M. K. Oberthaler, Phys. Rev. Lett. **92**, 230401 (2004).

[4] L. Bergé, Phys. Rep. **303**, 259 (1998).

[5] E. A. Kuznetsov and F. Dias, Phys. Rep. **507**, 43 (2011).

[6] A. Desyatnikov, A. Maimistov, and B. Malomed, Phys. Rev. E **61**, 3107 (2000).

[7] D. Mihalache, D. Mazilu, L.-C. Crasovan, I. Towers, A. V. Buryak, B. A. Malomed, L. Torner, J. P. Torres, and F. Lederer, Phys. Rev. Lett. **88**, 073902 (2002).

[8] F. Maucher, N. Henkel, M. Saffman, W. Królikowski, S. Skupin, and T. Pohl, Phys. Rev. Lett. **106**, 170401 (2011).

[9] I. Tikhonenkov, B. A. Malomed, and A. Vardi, Phys. Rev. Lett. **100**, 090406 (2008).

[10] Y. V. Kartashov, B. A. Malomed, and L. Torner, Rev. Mod. Phys. **83**, 247 (2011).

[11] E. L. Falcão-Filho, C. B. de Araújo, G. Boudebs, H. Leblond, and V. Skarka, Phys. Rev. Lett. **110**, 013901 (2013).

[12] L. Torner, S. Carrasco, J. P. Torres, L.-C. Crasovan, and D. Mihalache, Opt. Commun. **199**, 277 (2001).

[13] L. Torner and Y. V. Kartashov, Opt. Lett. **34**, 1129 (2009).

[14] B. B. Baizakov, B. A. Malomed, and M. Salerno, Phys. Rev. A **70**, 053613 (2004).

[15] D. Mihalache, D. Mazilu, F. Lederer, Y. V. Kartashov, L.-C. Crasovan, and L. Torner, Phys. Rev. E **70**, 055603 (2004).

[16] D. Mihalache, D. Mazilu, F. Lederer, B. A. Malomed, Y. V. Kartashov, L.-C. Crasovan, and L. Torner, Phys. Rev. Lett. **95**, 023902 (2005).

[17] Y. C. Zhang, Z. W. Zhou, B. A. Malomed, and H. Pu, Phys. Rev. Lett. **115**, 253902 (2015).

[18] J. R. Abo-Shaeer, C. Raman, J. M. Vogels, and W. Ketterle, Science **292**, 476 (2001).

[19] O. Mandel, M. Greiner, A. Widera, T. Rom, T. W. Hänsch, and I. Bloch, Nature (London) **425**, 937 (2003).

[20] A. Vasara, J. Turunen, and A. Friberg, J. Opt. Soc. Am. A **6**, 1748 (1989).

[21] J. Arlt and K. Dholakia, Opt. Commun. **177**, 297 (2000).

[22] R. Fischer, D. N. Neshev, S. Lopez-Aguayo, A. S. Desyatnikov, A. A. Sukhorukov, W. Krolikowski, and Y. S. Kivshar, J. Mater. Sci. Mater. Electron. **18**, S277 (2007).

[23] R. Fischer, D. N. Neshev, S. Lopez-Aguayo, A. S. Desyatnikov, A. A. Sukhorukov, W. Krolikowski, and Y. S. Kivshar, Opt. Express **14**, 2825 (2006).

[24] X. Wang, Z. Chen, and P. G. Kevrekidis, Phys. Rev. Lett. **96**, 083904 (2006).

[25] Y. V. Kartashov, A. Ferrando, A. A. Egorov, and L. Torner, Phys. Rev. Lett. **95**, 123902 (2005).

[26] Y. V. Kartashov, V. A. Vysloukh, and L. Torner, Phys. Rev. Lett. **94**, 043902 (2005).

[27] Y. V. Kartashov, R. Carretero-González, B. A. Malomed, V. A. Vysloukh, and L. Torner, Opt. Express **13**, 10703 (2005).

[28] Liangwei Dong, Hui Wang, Weidong Zhou, Xiaoyu Yang, Xiang Lv, and Haiyun Chen, Opt. Express **16**, 5649 (2008).

[29] Fangwei Ye, Yaroslav V. Kartashov, B. Hu and L. Torner, Opt. Express **17**, 11328 (2009).

[30] V. Galitski and I. B. Spielman, Nature (London) **494**, 49 (2013).

[31] T. D. Stanescu, B. Anderson, and V. Galitski, Phys. Rev. A **78**, 023616 (2008).

[32] Y. J. Lin, K. Jimenez-Garcia, and I. B. Spielman, Nature (London) **471**, 83 (2011).

[33] J. Dalibard, F. Gerbier, G. Juzeliūnas, and P. Ohberg, Rev. Mod. Phys. **83**, 1523 (2011).

[34] X. Q. Xu and J. H. Han, Phys. Rev. Lett. **107**, 200401 (2011).
[35] G. J. Conduit, Phys. Rev. A **86**, 021605(R) (2012).
[36] C. Wang, C. Gao, C. M. Jian, and H. Zhai, Phys. Rev. Lett. **105**, 160403 (2010).
[37] V. Achilleos, D. J. Frantzeskakis, P. G. Kevrekidis, and D. E. Pelinovsky, Phys. Rev. Lett. **110**, 264101 (2013).
[38] Y. Xu, Y. Zhang, and B. Wu, Phys. Rev. A **87**, 013614 (2013).
[39] H. Sakaguchi, B. Li, and B. A. Malomed, Phys. Rev. E **89**, 032920 (2014).
[40] Y. V. Kartashov, V. V. Konotop, and D. A. Zezyulin, Phys. Rev. A **90**, 063621 (2014).
[41] J. Yang and T. I. Lakoba, J. Stud. Appl. Math., **120**, 265 (2007).
[42] S. L. Xu, M. R. Belić, G. Zhou, J. He, and L. Xue, Opt. Express **25**, 9094 (2017).